Confinement and MHD stability in the Large Helical Device

O.Motojima 1), K.Ida 1), K.Y.Watanabe 1), Y.Nagayama 1), A.Komori 1), T.Morisaki 1), B.J.Peterson 1), Y.Takeiri 1), K.Ohkubo 1), K.Tanaka 1), T.Shimozuma 1), S.Inagaki 1), T.Kobuchi 1), S.Sakakibara 1), J.Miyazawa 1), H.Yamada 1), N.Ohyabu 1), K.Narihara 1), K.Nishimura 1), M.Yoshinuma 1), S.Morita 1), T.Akiyama 1), N.Ashikawa 1), C.D.Beidler **2)**, M.Emoto 1), T.Fujita **3)**, T.Fukuda **4)**, H.Funaba 1), P.Goncharov **5)**, M.Goto 1), T.Ido 1), K.Ikeda 1), A.Isayama **3)**, M.Isobe 1), H.Igami 1), K.Ishii **6)**, K.Itoh 1), O.Kaneko 1), K.Kawahata 1), H.Kawazome **7)**, S.Kubo 1), R.Kumazawa 1), S.Masuzaki 1), K.Matsuoka 1), T.Minami 1), S.Murakami **8)**, S.Muto 1), T.Mutoh 1), Y.Nakamura 1), H.Nakanishi 1), Y.Narushima 1), M.Nishiura 1), A.Nishizawa 1), N.Noda 1), T.Notake **9)**, H.Nozato **4)**, S.Ohdachi 1), Y.Oka 1), S.Okajima **10)**, M.Osakabe 1), T.Ozaki 1), A.Sagara 1), T.Saida **11)**, K.Saito 1), M.Sakamoto**12)**, R.Sakamoto 1), Y.Sakamoto **3)**, M.Sasao **11)**, K.Sato 1), M.Sato 1), T.Seki 1), M.Shoji 1), S.Sudo 1), N.Takeuchi **9)**, H.Takenaga **3)**, N.Tamura 1), K.Toi 1), T.Tokuzawa 1), Y.Torii **13)**, K.Tsumori 1), T.Uda 1), A.Wakasa **14)**, T.Watari 1), I.Yamada 1), S.Yamamoto **13)**, K.Yamazaki 1), M.Yokoyama 1), Y.Yoshimura 1)

1) National Institute for Fusion Science, 322-6 Oroshi-cho, Toki-shi, 509-5292, Japan
2) Max-Planck Institut fuer Plasmaphysik, Greifswald D-17491, Germany
3) Japan Atomic Energy Research Institute, Naka, 311-0193, Japan
4) Graduate School of Engineering, Osaka University, Suita, Osaka 565-0871,
5) Department of Fusion Science, School of Mathematical and Physical Science, Graduate University for Advanced Studies, Hayama, 240-0193, Japan
6) Plasma Research Center, University of Tsukuba, Tsukuba, 305-8577, Japan
7) Graduate School of Energy Science, Kyoto University, Uji 611-0011, Japan
8) Department of Nuclear Engineering, Kyoto University, Kyoto 606-8501, Japan
9) Department of Energy Engineering and Science, Nagoya University, 464-8603, Japan
10) Chubu University, Kasugai, Aichi, 487-8501, Japan
11) Graduate School of Engineering, Tohoku University, Sendai, 980-8579, Japan
12) Research Institute for Applied Mechanics, Kyushu University, Kasuga, 816-8580, Japan
13) Institute of Advanced Energy, Kyoto University, Uji, 611-0011, Japan
14) Graduate School of Engineering, Hokkaido University, Sapporo 060-8628, Japan

e-mail contact of main author: motojima@LHD.nifs.ac.jp

Abstract.

The Large Helical Device (LHD) is a heliotron device with l = 2 and m = 10 continuous helical coils with a major radius of 3.5 – 3.9 m, a minor radius of 0.6 m, and a toroidal field of 0.5 – 3 T, which is a candidate among toroidal magnetic confinement systems for a steady state thermonuclear fusion reactor. There has been significant progress in extending the plasma operational regime in various plasma parameters by neutral beam injection (NBI) with a power of 13MW and electron cyclotron heating (ECH) with a power of 2MW. The electron and ion temperature have reached up to 10 keV in the collisionless regime and the maximum electron density, the volume averaged beta value and stored energy are 2.4×10^{20} m^{-3}, 4.1% and 1.3 MJ, respectively. In the last two years, intensive study of the MHD stability providing access to the high beta regime and of healing of the magnetic island in comparison with the neoclassical tearing mode in tokamaks has been conducted. Local Island Divertor (LID) experiments also have been done to control the edge plasma aimed at confinement improvement. As for transport study, the transient transport analysis was executed for the plasma with an internal transport barrier (ITB) and a magnetic island. The high ion temperature plasma was obtained by adding impurities to the plasma to keep the power deposition to the ions reasonably high even at very low density. By injecting 72kW of ECH power, the plasma was sustained for 756 second without serious problems of impurities or recycling.

1. Introduction

A heliotron type device is a probable candidate among toroidal magnetic confinement systems as a thermonuclear fusion reactor under steady-state operation because it can confine plasma with only external coils and utilizing a well-defined divertor configuration. Compatibility between magnetohydrodynamics (MHD) stability and good confinement is one of the crucial issue in the Heliotorn device, because there exists a trade off between the magnetic well and small drift of helicaly trapped particles from the magnetic flux surface [1]. When the plasma is shifted outward, the high β plasma will not be achieved because of the reduced confinement and the limited heating power, not because of the MHD instability. Ideal MHD instabilities universally have the potential for strongly limiting the operational regime of the plasma parameters in high β regime. In tokamaks, it is well known that the operational β limits are quite consistent with the theoretical predictions of ideal linear MHD theory [2,3]. On the contrary, in helical plasmas, a limited number of experimental research into the effects of pressure driven ideal MHD instabilities on the operational beta range has been reported, for examples, on Heliotorn DR [4], the compact helical system (CHS) [5] and the Large Helical Device[6].

Large Helical Device (LHD) is a superconducting heliotron device (poloidal period number L = 2, and toroidal period number M = 10) with a major radius of R_{ax} =3.5 – 4.1 m, an average minor radius of 0.6 m, magnetic field up to 3T, and heating neutral beam with negative ions with a beam energy of 150 – 180 keV[7,8] with a radius of tangency, R_{T_NBI} of 3.65m - 3.7m. The high β experiment is done in the inward shifted configuration, where the confinement is good (and the β limit is low) enough to study the β limit in a heliotron device. Because the plasma pressure is still marginal for the β limit even in the inward shifted configuration, the improvement of confinement is required. The extended operation regimes, the development of control techniques and understanding of transport, especially in the plasma with an internal transport barrier[9-12] are discussed in this paper.

2.MHD study

2.1. High beta experiment

The operational highest beta value has been expanded from 3.2% to 4% in the last two years by increasing the heating capability and exploring a new magnetic configuration with a higher aspect ratio by changing the pitch parameter of the helical coil, γ(=n/2·a/R), from 1,254 to 1.22[13]. This new configuration with higher aspect ratio is characterized by a smaller volume and smaller Shafranov shift than the standard configuration as seen in Fig1. Although the MHD stability properties are expected to be even worse according to ideal MHD theory in this configuration (γ = 1.22) than in the so-called standard configuration (γ = 1.254), the smaller shift is considered to contribute to the central deposition of the neutral beam and hence the reduction of the direct loss of the beam by keeping the magnetic axis close to the tangential radius of the neutral beam (indicated by the shaded region in Fig.1) at higher beta.

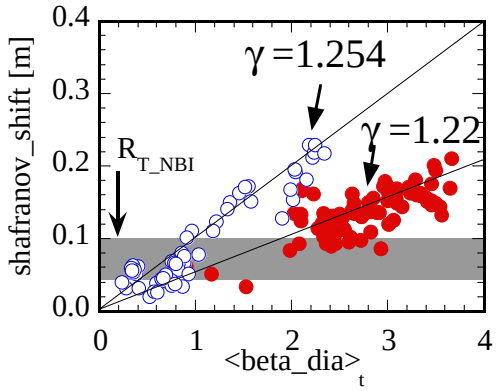

Fig.1 Shafranov shift as a function of beta value for the configurations of R_{ax} =3.6 and γ =1.254 and γ =1.22.

Figure 2(a) shows typical MHD activities in a typical high-beta discharge with a magnetic axis of 3.6 m and a magnetic field of 0.45 T, respectively. As the electron density is increased by the gas puff, the volume averaged β value estimated from the stored energy measured with a diamagnetic loop, $\langle b_{dia} \rangle$, increases and reaches 4% at 1.12sec. Here the $\langle b_{dia} \rangle$ is the diamagnetic beta value defined as $4\mu_0/3 \cdot W_{dia}/(B_{av0}{}^2 V_{p0})$, where W_{dia} is the diamagnetic energy. The B_{av0} and V_{p0} are the averaged toroidal magnetic field inside the

plasma boundary and plasma volume, respectively, and both of them are estimated under vacuum condition. The β value estimated from the kinetic stored energy based on the measured electron temperature and density profiles is 3.3% assuming Z_{eff} = 1, while the β value due to beam pressure evaluated with the FIT[14] code is 1.5%. Here, it should be noticed that the β values estimated with kinetic measurements and with beam pressure calculation have relatively large uncertainties due to the lack of precise measurements of ion density and temperature profiles and due to the difficulty in evaluating the accurate orbit loss of high energy ions in the low magnetic field of 0.45T. The m/n = 1/1 and 2/3 modes of the magnetic fluctuations excited in the edge region are dominantly observed in this discharge. Here m and n are the poloidal and toroidal mode-numbers of the magnetic fluctuations, respectively. The m/n = 1/1 and 2/3 modes grow from 0.5s and their amplitudes increase with $<\beta_{dia}>$. However, when $<\beta_{dia}>$ exceeds a certain value at 1.14 s, the m/n = 1/1 mode is frequently interrupted.

The equilibrium reconstruction and stability analysis are done for this discharge by the 3-D MHD equilibrium code VMEC[15]. Figure 2(b) shows the experimentally observed beta gradients at ρ=0.9 in the R_{ax} =3.6m and γ = 1.22 configuration, where the rotational transform is estimated to be unity, as a function of $<\beta_{dia}>$. The data were obtained in 0.45T to 1.75T operation. Here the β gradients are evaluated with kinetic pressure measurements and volume averaged β is given by diamagnetic loop measurements. The solid line in Fig.2(b) denote a contour of the low-n (m/n =1/1) ideal MHD modes (with global mode structure) with $\gamma_{low\text{-}n}/\omega_A$= $0.5\text{x}10^{-2}$ and $1.0\text{x}10^{-2}$ for currentless equilibria. The growth rate is calculated by a MHD stability analysis code (TERPSICHORE [16]). Here $\omega_A = v_{A0}/R_0$, v_{A0} and R_0 are the Alfven velocity and the major radius at the magnetic axis. The dotted lines are the stability boundary of Mercier modes (with a highly localized mode structure / high-m limit) [17]. The change of the gradients are observed around $<\beta_{dia}>$=1.5%, which corresponds to Mercier unstable region. However, the observed beta gradients at ρ=0.9 increases with increasing beta up to $<\beta_{dia}>$ = 4%. Here, the electron temperature profiles measured with a multi-channel YAG Thomson scattering often show a local flattening at the rational surface, which is not included in the analysis using VMEC discussed above[18].

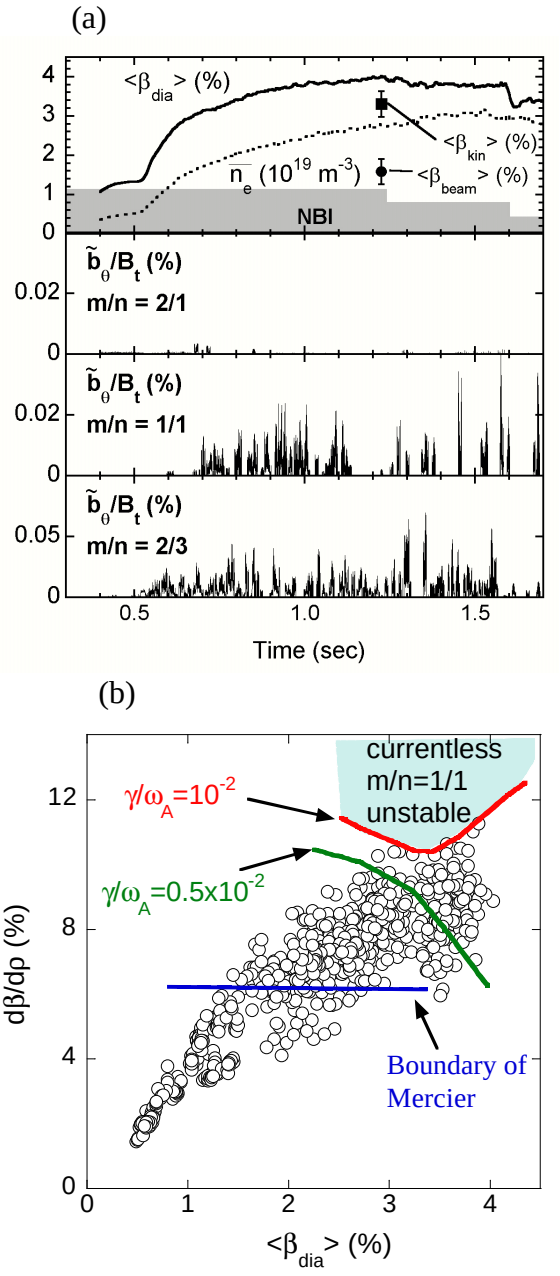

Fig.2 (a) Time evolution of averaged electron density and averaged β value and magnetic fluctuation of m/n mode and (b) kinetic beta gradients at ρ=0.9 (ι/2π = 1) in <β>-dβ/dρ diagram.

An important subject of investigation is the effect of β on confinement. Figure 3 shows the improvement factor (H_{ISS}) of the global energy confinement time evaluated with the diamagnetic flux measurements on the ISS95 (International Stellarator Scaling 1995) empirical scaling[19] as a function of $<\beta_{dia}>$. A serious degradation of a global energy confinement time has not been observed up to $<\beta_{dia}>$ ~4%, and the enhancement factor is gradually reduced in $<\beta_{dia}>$ >2%. This gradual decrease of the enhancement factor is thought mainly to be due to the increase of the electron density (and plasma collisionality) to achieve a high β plasma, not due to MHD stability, since the gradual decrease of the enhancement factor is also observed in the plasma with low β values s low less than 1.5%). This is due to the weaker density dependence of the energy confinement time (weaker temperature dependence on thermal diffusivity) at higher plasma collisionality[20], while the density dependence of the energy confinement time of $n_e^{0.5}$ (Gyro-Bohm type scaling) is assumed to be unchanged over a wide range of the collisionality in the ISS95.

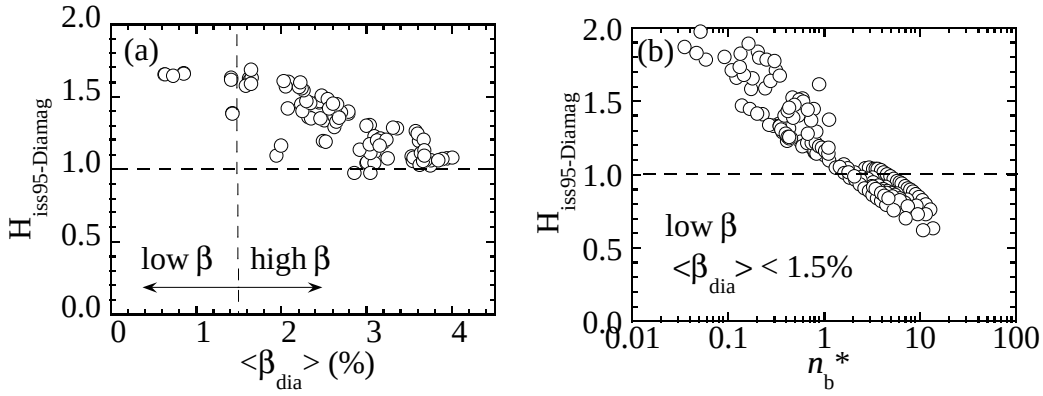

Fig.3 The improvement factor of effective energy confinement as a function of (a) beta value for the plasma with R_{ax}=3.6m, B=0.45-1.75T? and γ = 1.22 and (b) collisionality normalized by bounce frequency of banana orbit particles for the plasma with R_{ax}=3.6m, B=1.5-2.75T and γ = 1.254.

2.2. Healing of Magnetic island

The suppression of the growth of the magnetic island at a rational surface in the high β regime is the other important issue of MHD, which has been considered to be a serious problem in tokamak plasmas known as the neoclassical tearing mode. In LHD, where the magnetic shear is negative, the magnetic island is healed rather than growing in contrast to the neoclassical tearing mode. The experiment in the plasma with an n/m = 1/1 perturbation field clearly shows that this healing effect becomes more effective as the conductivity or the beta is increased[21,22]. The bootstrap current and Pfirsch-Schluter current are considered as candidates to cause healing of the magnetic island[23], however, the magnitude of these currents in the plasma with a magnetic island is too small to be sufficient for healing the magnetic island. Therefore the characteristic of magnetic island healing is considered to be one of the advantages of a heliotron configuration, because it gives more tolerance for the error magnetic field, which is difficult to be eliminated completely.

Figure 4(a) shows time evolution of the T_e profile at $\phi=136^o$ after the hydrogen pellet injection in the case of R_{ax}=3.6 m. This is a typical evidence of 'healing' events. The island appears after the pellet injection, but the island width (w) is reduced as the temperature increases. Finally, the T_e profile returns to that before the pellet injection, and the island disappears. The island width in the plasma depends on the plasma parameters. In this experiment, it is observed that the magnetic island width decreases as T_e or beta increases. Figure 4(c) shows that the island width in vacuum is increased as the n=1 coil current (I_N) increases, but the island in the plasma suddenly appears when it surpasses the threshold of the current[21,24]. This is another aspect of 'healing'. Here, the coil current is normalized to B_{ax}. The threshold level (I_N^*) is increased as the beta increases, as shown in Fig.4(c).

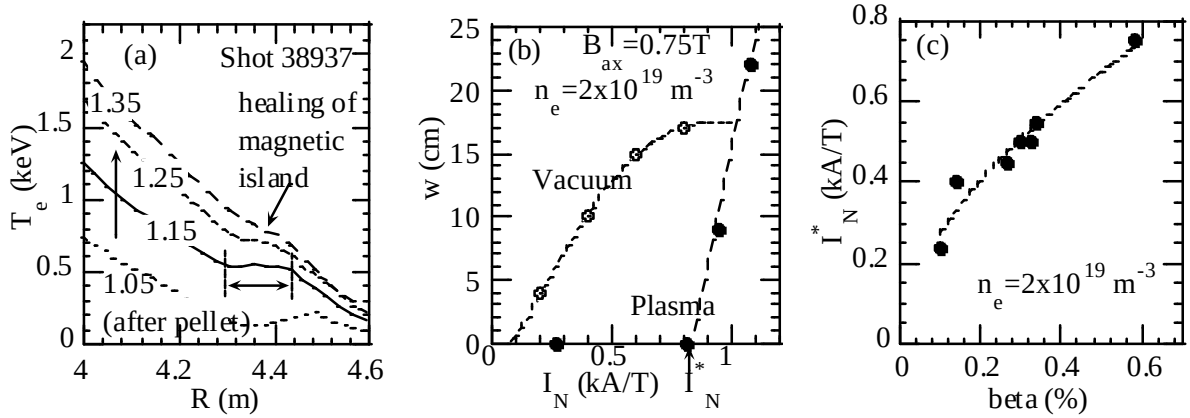

Fig.4 Time evolution of the T_e profile with the n=1 external field. (b) Normalized coil current vs. island width (w) in vacuum (open circles) and in plasma (closed circles). (c) beta vs. threshold of the normalize coil current.

3. Extended operation regime in LHD

3.1 Edge control by Local island divertor

A local island divertor (LID) has been installed in the LHD plasma to increase edge pressure gradients to achieve better energy confinement time. As discussed in 2.2, LHD plasma shows a weaker density dependence of the global energy confinement time than the ISS95 scaling at higher density. This saturation at the higher density should be due to the lower collisionality near the plasma edge, because a stronger gas puff applied to achieve the high density causes a flat density profile. Therefore it is considered to be important to reduce the edge density keeping the lower collisionality and improve energy transport at the edge to achieve a good energy confinement time. The LID is a kind of pumped limiter inserted inside the n/m=1/1 magnetic island produced at the plasma edge. Since LID head is inserted to the middle of the O-point of the magnetic island, the core plasma does not touch the limiter and the outward heat and particle fluxes do not directly go to the front of the limiter but flows to the backside of the LID limiter along the field lines across the separatrix [25,26].

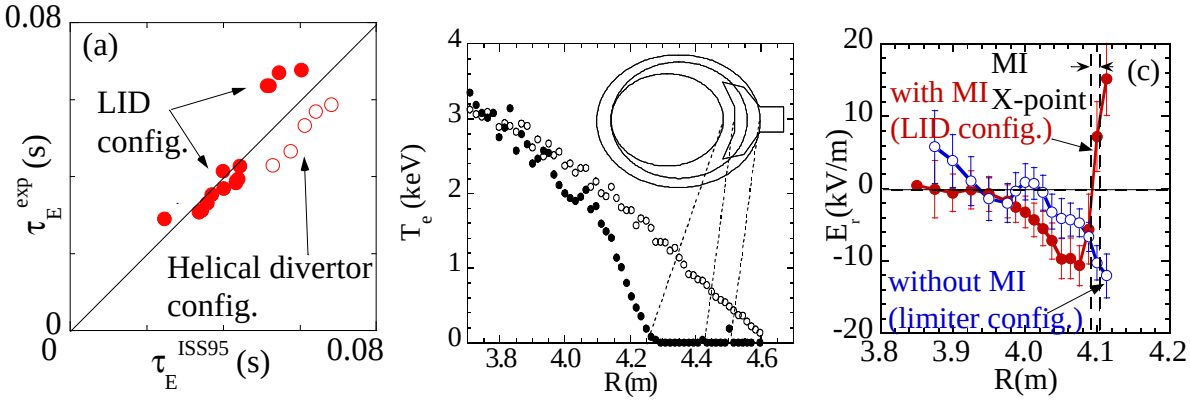

Fig.5 (a)comparison of energy confinement time observed to the that predicted by the ISS95 scaling and (b) radial profiles of electron temperature for the plasma with helical divertor configuration (open circles) and LID configuration (closed circles) in LHD and (c) radial profiles of radial electric field with magnetic island (LID configuration) and without magnetic island (limiter configuration).

In the present experiment with LID as is mentioned above, a factor of ~1.2 improvement of the energy confinement time has been observed over the ISS95 at higher electron density (larger energy confinement time) regime as seen in Fig5(a). This amount of reduced enhancement of energy confinement time is thought to be due to the increase of the

edge temperature gradient as seen in Fig5(b). Although the minor radius of the plasma is reduced by inserting the LID head into the magnetic island produced by an n/m = 1/1 external perturbation field, the core electron temperature does not drop because of the larger electron temperature. At the moment, the experiments are restricted to the relative low density (due to technical reason related to the plasma operation), where the absolute value of the energy confinement is low, because the pumping exceeds the capability of efficient central fuelling. In order to achieve the improvement at higher density, more efficient central particle fuelling such as due to beam fuelling or a pellet with a higher speed is required. Another characteristic of the plasma with LID configuration is low radiation level. A significant impurity shielding is observed in the plasma with the LID configuration in the Ne puff experiments. In this discharges, there is a large positive radial electric field observed at the X-point of the magnetic island in the LID configuration[Fig5(c)]. This positive radial electric field contributes to the exhaust of impurities and prevents the radiation collapse, while the negative electric field and its shear contribute to the improvement of heat transport.

3.2 Control of radial electric field by shift of magnetic axis

A change in the magnitude and radial profiles of the helical ripples will be the most straightforward tool to control the radial electric field. The reason is that the radial electric field in LHD is determined by the ambipolar condition of ion flux and electron flux that are trapped in helical ripples[27]. In LHD, the radial profiles of the helical ripples can be controlled by the shift of the magnetic axis from 3.9m to 3.5m.[28] .

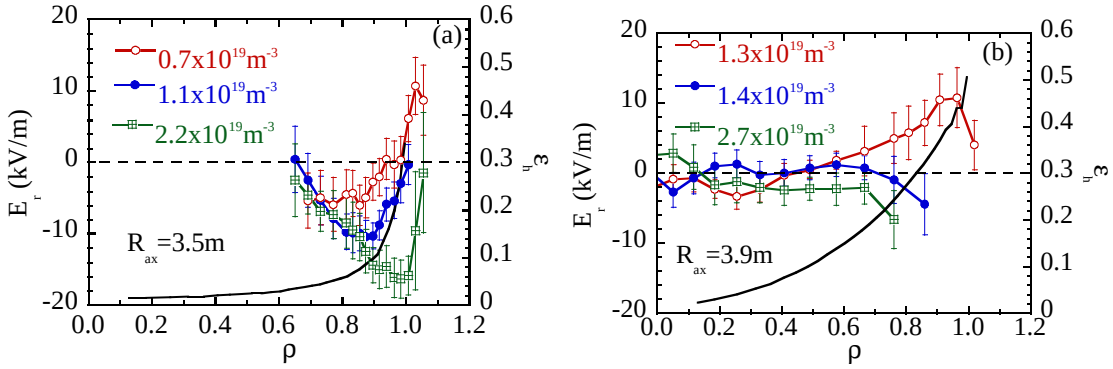

Fig.6 (a) Radial profiles of radial electric field for the plasma with a magnetic axis of (a) 3.5m (inward shift configuration) and (b) 3.9m (outward shift configuration)

Figure 6 shows the radial profiles of the radial electric field for the ion root (large neoclassical flux with negative E_r in the high collisionality regime), electron root (small neoclassical flux with positive E_r in the low collisionality regime) and the transition regime (between ion root and electron root) for various configurations with different helical ripple profiles. When the helical ripple increases gradually towards the plasma edge (R_{ax}=3.9m), the electron root region extends to half of the plasma minor radius and the radial electric field shear produced is relatively weak. However, when the helical ripple increases sharply at the plasma edge (R_{ax}=3.5m), the electron root region is localized at the plasma edge and strong radial electric field shear is produced. These results show that a strong magnetic field shear can be obtained at the plasma edge by shifting the magnetic axis inward rather than shifting the magnetic axis outward, where the electron root condition becomes achievable even at higher collisionality.

The electron density at the transition from ion root to electron root is 0.7 x $10x^{19}m^{-3}$ for the plasma with the magnetic axis of 3.5m, while it is 1.3 x $10^{19}m^{-3}$ for the plasma with the magnetic axis of 3.9m. The difference in critical electron density can be explained by the

differences in the magnitude of helical ripples and these characteristics are consistent with the prediction by neoclassical theory[29,30].

3.3 Density limit and radiation collapse

It is important to study the mechanism of radiation collapse to extend the density limit, since the plasma is terminated by the radiation collapse at the density limit. The radial electric field is expected to be negative in the high density limit. In the latest experimental campaign in LHD, line-averaged densities of up to 1.6×10^{20}m^{-3} have been sustained for more than 0.7 s by 11 MW neutral beam injection using gas puff fuelling. In addition, using multiple hydrogen pellet injection, the density has been increased to 2.4×10^{20}m^{-3} transiently.

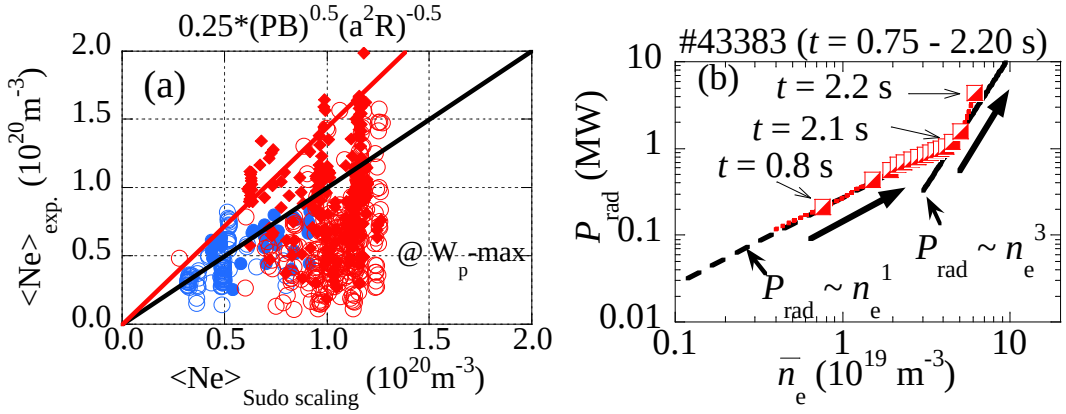

Fig.7. Comparison of achieved electron density to Sudo scaling and (b) total radiation power as a function of electron density.

Data from the most recent campaign also shows a limit which exceeds the Sudo limit [31] by a factor of approximately 1.4 as is seen in Fig.7(a). At the radiation collapse the thermal instability occurs, where the total radiation sharply increases because of the increase of cooling rate of impurities associated with the low edge temperature below 0.15keV at r = 0.9 regardless of the input power and plasma density[20].When the thermal instability starts, the total radiation power P_{rad} is proportional to $\bar{n}_e^{\,3}$, while it usually is proportional to $\bar{n}_e$ as demonstrated in Fig.7(b).

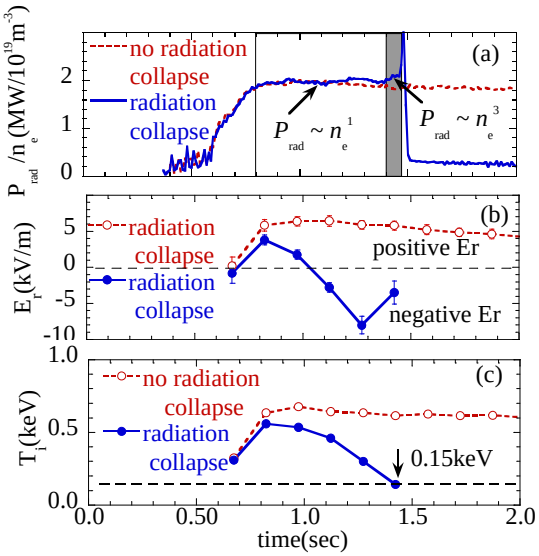

Fig.8 Time evolution of (a) normalized total radiation power, (b) radial electric field, (c) ion temperature at ρ = 0.9 for the discharges with and without radiation collapse.

The spontaneous increase of density and radiation power (which is proportional to $\bar{n}_e$) precedes the thermal instability, especially in the plasma with higher impurity concentration. In order to study this spontaneous density increase before the radiation collapse, a short Ne puff was applied to the early phase of the discharges[28]. When the short Ne puff is applied to the early phase of the discharge with the pulse width of t = 0.5 – 0.68s, there is no spontaneous density increase and

no radiation collapse as seen in Fig.8. In contrast, by slightly increasing the pulse width of Ne puff (t=0.5-0.7s), a clear spontaneous increase of radiation power and density is observed, although the Ne puff is already turned off.

The radial electric field at ρ = 0.9 starts to be more negative 0.5 sec before the radiation collapse, where the radiation loss due to NeVI and NeVII is maximum. The radial electric field becomes more and more negative until the radiation collapse. The change of radial electric field to more negative is due to the increase of collisionality (increase of electron density and decrease of temperature). When the radial electric field becomes more negative, the negative radial electric field causes the increase of impurity influx, because the exhausting effect by positive radial electric field disappears. In the discharge without radiation collapse, the radial electric field remains positive with no increase of electron density and radiation power. The ion temperature shows a significant drop to 0.15 keV and the thermal instability causing the radiation collapse starts. The role of positive electric field in preventing the spontaneous increase of the electron density and impurity radiation demonstrated in this experiment is also important in the LID configuration, because strong positive radial electric field is produced at the plasma edge as described in 3.1.

3.4 Achievement of high ion temperature with NBI

At present, LHD has three tangential neutral beams lines with negative-ion-sources, of which are designed to have a high energy of around 180keV. They are effective tools for the experiment, but primarily contribute to the electron heating rather than the ion heating. To increase the ion temperature up to 10keV and to investigate the property of high ion temperature plasma, the experiments using the high-Z plasmas have been done with Ar- and/or Ne-gas fuelling to increase beam absorption and energy deposition to ions in low-density plasmas. Intensive Ne- and/or Ar glow discharge cleaning was applied to reduce the wall-absorbed hydrogen and increase the concentration of Ne and/or Ar ions. As a result, the ion temperature increases with an increase in the ion heating power normalized by the ion density, and the highest ion temperature obtained in LHD has increased from 5 keV to 10 keV in the last two years[32,33]. However, plasma with large concentration of high-Z impurity is not be relevant for the future research aimed at nuclear fusion because of the large dilution of the fuelling. Therefore this is intended as a preparatory experiment to study the property of high ion temperature plasma up to 10keV and to demonstrate the high capability of LHD as a magnetic confinement device, before the installation of a neutral beam with the energy of 40 keV for the purpose of ion heating, which is planned to be installed in LHD in the near future.

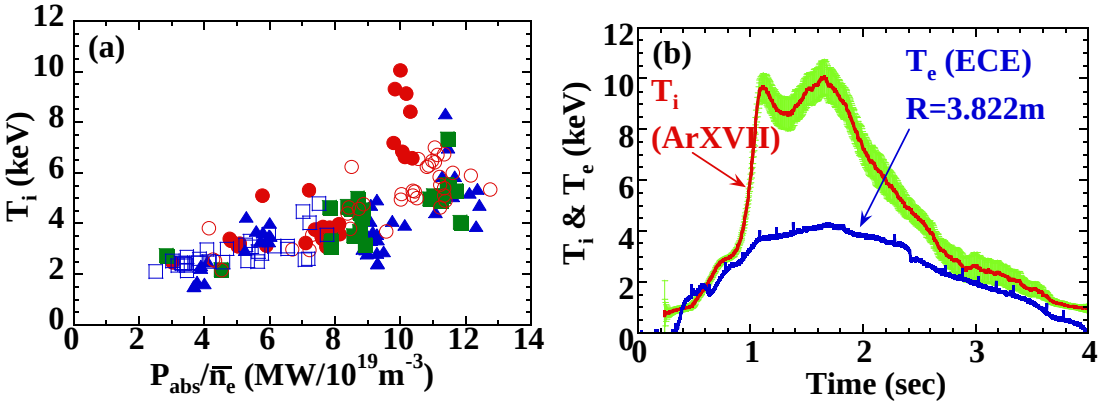

Fig. 9 (a) Ion temperature as a function of the direct ion heating power normalized by the ion density in the plasma with Ar- and Ne-puff and (b) time evolution of electron and ion temperature in a low-density high-Z plasma.

The ion temperature increases with increasing normalized ion heating power in the plasma with Ar- and Ne-puff as seen in Fig.9(a). No distinct saturation has been observed. Figure 9(b) shows the time evolutions of ion and electron temperatures in the plasma with Ar-puff at t=0.5s. After an increase in the electron density due to the Ar gas-puff, the central ion temperature, measured with the Doppler broadening of an X-ray line of ArXVII, rapidly increases as the density decreases with the addition of NBI power, and stays at high values. The ion temperature reaches 10 keV at around t=1.65s with an injection power of 12.2 MW, around 30 % of which is absorbed at an electron density of $0.37 \times 10^{19} m^{-3}$. The electron temperature is also increased up to 4.3 keV, and, however, is much lower than the ion temperature. The observed beam slowing-down time after the NBI-off is as long as 1.2 s probably due to both the low electron density and the high electron temperature, and the ion and electron temperatures show an extremely slow decay after the beam turn-off.

3.5 Long pulse operation with ECH

In the LHD, steady-state plasma heating by electron cyclotron (EC) wave with 72kW and ICRF with 500kW was achieved during 756 and 150 sec, respectively. A EC heated plasma with time-averaged radiation temperature of 240eV and density of less than $1 \times 10^{18} m^{-3}$ was obtained. As for an ICRF heated plasma, plasma with electron and ion temperature of 2 keV and density of $6 \times 10^{18} m^{-3}$ were sustained until the discharge was terminated by increase in radiation loss.

4 Transport study

4.1 Property of particle transport

Hollow density profiles are often observed in LHD, which is in contrast to the peaked density profiles observed in tokamak plasmas. A hollow profile even in the steady state suggests the existence of outward convective velocity in the core region, because the density profiles should be flat in the steady state in the plasma, where most of the particle source is localized at the plasma edge. In order to study the parameter dependence of diffusion and convective velocity in the plasma, a modulated gas puff is applied to the plasma [34].

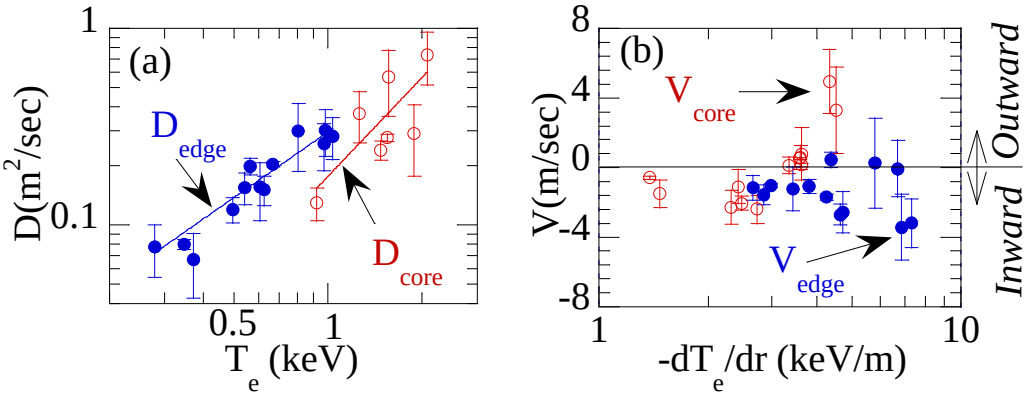

Fig.10 (a) Electron temperature dependence of diffusion coefficient and (b) convective velocity as a function of the temperature gradient.

The diffusion coefficient increases as the temperature is increased as seen in Fig10(a). The temperature dependence of the diffusion coefficient is $T_e^{1.7+-0.9}$ and $T_e^{1.1+-0.14}$ in the core ($\rho < 0.7$) and the edge ($\rho > 0.7$), respectively, both values are close to that expected by gyro-Bohm scaling of $T_e^{1.5}$. The dependence of edge diffusion on magnetic field is measured to be

B^{-2}, which is also consistent with the prediction of gyro-Bohm scaling. These characteristics are supported by the fluctuation measurements using CO_2 laser scattering. Figure 10(b) shows that the convective velocity in the core becomes more positive, while the convective velocity in the edge becomes more negative as the temperature gradient is increased, which results in the density profile becoming more hollow associated with the increase of the temperature gradients at higher heating power.

4.2 Electron transport

An electron internal transport barrier (ITB) is characterized with the peaked electron temperature profile associated with the transition from ion root to electron root observed in the NBI sustained plasmas with centrally focused ECH [9-12]. The characteristics of the formation of the ITB depend on the direction of the neutral beam[35]. Figure 11(a) shows the increment of the electron temperature, ΔT_e, at the plasma center by ECH power as a function of ECH power normalized by the electron density. The threshold power for the transition to the ITB plasma is clearly observed in the plasma with counter(CNTR) NBI in the direction that the beam driven current increases the rotational transform in the plasma. This is in contrast to that the central T_e increases almost linearly with the ECH power and no clear threshold power for the transition to ITB plasma is observed in the plasma with co(CO) NBI in the direction of decreasing rotational transform by beam driven current. The differences in the characteristics are due to the differences in rotational transform i and not due to the differences in the deposition profile. In the plasma with CNTR NBI, the rational surface of $i/2\pi=1/2$ is located at half of the plasma minor radius, while the plasma with CO NBI has no $i/2\pi=1/2$ rational surface because of the increase of central rotational transform above 0.5. As the magnetic axis shifts outward, the rational surface of $i/2\pi=1/2$ moves toward the plasma edge and always exists in the plasma, regardless of the direction of the NBI, the difference in characteristics of the ITB between CO NBI and CNTR NBI becomes small.

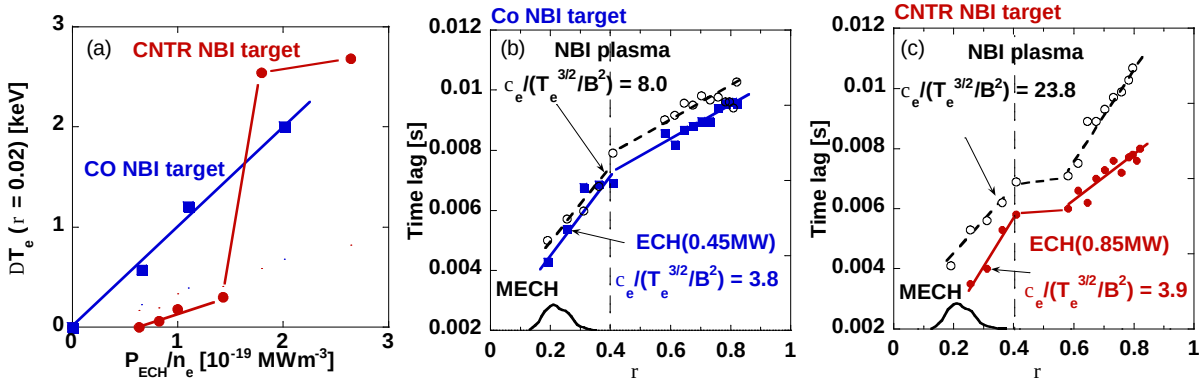

Fig.11 (a) Electron temperature increases at the center and peripheral are plotted as a function of density-normalized ECH power and time lag of ECE signals from MECH is plotted versus normalized minor radius for (b) CNTR NBI heated plasma and (c) Co NBI heated plasma. Electron heat diffusivities estimated from heat pulse propagation velocity are also indicated in the figures.

The time lag that gives the maximum correlation at each position is plotted in Fig. 11(b)(c), together with power deposition profile of the modulated electron cyclotron heating (MECH) calculated by a ray tracing code. The incremental electron heat diffusivity, c_e, is evaluated from the slope of the time lag. The heat diffusivity normalized by the gyro-Bohm scaling $T_e^{3/2} / B^2$ reduced from 8.0 to 3.8 $m^2 \cdot s^{-1} \cdot keV^{3/2} \cdot T^2$ with the increase of ECH power, which indicates an improvement of confinement. The flattening of the time lag observed at r = 0.4 - 0.55 in Fig. 11 (c) is due to the appearance of a magnetic island at the rational surface of $i/2\pi=1/2$.

Another approach to estimate the incremental electron thermal diffusivity is cold pulse propagation induced by a tracer encapsulated solid pellet (TESPEL) [36] ablated near the plasma edge. The thermal diffusivity can be derived with transient transport analysis using the perturbed heat transport equation[37,38]. Figure 12(a) shows the radial profiles of thermal diffusivity evaluated using cold pulse propagation, χ_{cp} and thermal diffusivity evaluated with power balance, χ_{pb}. The significant reduction of the electron thermal diffusivity inside the ITB (2 m^2/s inside and $10m^2/s$ outside ITB) is observed both in the χ_{cp} and χ_{pb}. The temperature dependence of the thermal diffusivity, α, where the electron thermal diffusivity is proportional to the temperature to the power of T_e as T_e^{α}, is an important parameter in the study of the plasma with an ITB. In L-mode, the parameter α is positive and typically it is 1.5, which is predicted from the gyro-reduced Bohm scaling and is also consistent with the scaling of energy confinement in LHD. If the parameter α stays positive, the formation of an ITB would never occur, because spontaneous increase of electron temperature during the formation of an ITB requires a negative α. The transient transport analysis with a cold pulse indicates the existence of $d\chi_e/dT_e$ and α can be derived from $d\chi_e/dT_e$ as $\alpha = (T_e/\chi_e)(d\chi_e/dT_e)$. As shown in Fig.12(b), the temperature dependence parameter, α, derived from the cold pulse propagation with transient transport analysis also shows the same trend. The temperature dependence is positive (α = 0.5 - 1.0) outside the ITB, while it becomes negative inside the ITB and decreases down to -3 towards the magnetic axis. The observation of negative α is considered to be the most significant evidence of an electron ITB in the plasma.

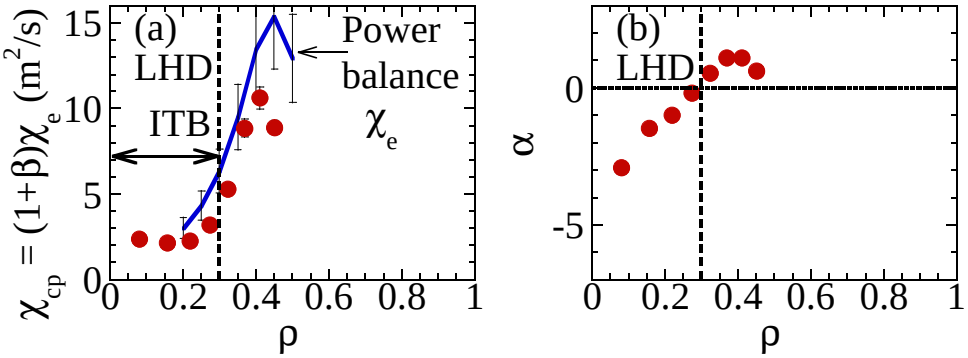

Fig.12 The radial profiles of the electron heat diffusivity and (b) the T_e dependence factor of χ_e , α , estimated by cold pulse propagation. The heat diffusivity estimated by power balance is also plotted.

5 Summary

In the inner shifted configuration where the β limit is expected to be low (1.5% in the Mercier limit), high beta plasma with $<\beta_{dia}>=4\%$ is obtained in the high aspect ratio configuration where the pitch parameter of helical coil, γ, is 1.22. The β values achieved significantly exceeds the linear MHD stability criteria, the Mercier limit and reaches to the region where the low-n (m/n =1/1) ideal MHD modes are predicted to be unstable. The difference in magnetic field configuration between a heliotron plasma and a tokamak plasma is positive shear and magnetic well in a tokamak and negative shear and magnetic hill in a heliotron plasma. The characteristic of magnetic island healing, which is considered to be advantagesous for a reactor, is due to the negative magnetic shear which is common in a heliotron configuration. This is in contrast to the tendency of magnetic islands to grow in tokamaks, where the magnetic field shear is typically positive. The negative magnetic shear is considered to contribute to the formation of an electron internal transport barrier[39,40]. The electron internal transport barrier is observed in a tokamak, when the magnetic shear changes its sign from positive to negative. In a heliotron plasma, where the magnetic field shear is negative, the electron internal transport barrier is usually observed with ECH heating in the electron root.

LID is now showing high capability as a powerful tool for edge control to achieve an improved confinement regime. It is an important role of the LHD project as a three dimensional currentless steady state magnetic confinement device to supply a high quality database for the plasma physics and sciences necessary to realize controlled nuclear fusion, which should be focused on 1) steady state physic, 2) high β physic, and 3) confinement improvement and edge control[39].

Acknowledgements

The comparison experiments investigating the mechanism of confinement improvement especially in the electron internal transport barrier has been performed under the collaboration between JT60U and LHD group. The author would like to thank the technical staff for their support of the LHD experiments.

References

[1] O.Kaneko et al., Phys. Plasma 9 (2002) 2020.
[2] M. Wakatani, Y. Nakamura and K.Ichiguchi, Fusion Eng. Design 15 (1992) 395.
[3] ITER Physics Basis, Nuclear Fusion 39 (1999) 2137.
[4] N. Yanagi et al, Nucl. Fusion 32 (1989) 1264.
[5] S. Okamura et al, Nucl. Fusion 30 (1999) 1337.
[6] K.Y. Watanabe et al, Fusion Sci. Tech. 46 (2004) 24.
[7] O.Motojima, et al., Nucl. Fusion 43 (2003) 1674.
[8] O.Motojima et. al., Fusion Science and Technology Vol 46 (2004) 1
[9] T.Shimozuma et al., Plasma Phys Control Fusion 45 (2003) 1183.
[10] K.Ida, et. al., Phys Rev Lett 91 (2003) 085003.
[11] Y.Takeiri et al., Phys. Plasma 10 (2003) 1788
[12] K.Ida, et. al., Phys plasmas 11 (2004) 2551
[13] K.Y. Watanabe et al, this conference.
[14] S. Murakami, Nuclear Fusion 36 (1996) 359.
[15] S.P.Hirshman, Phys. Fluids 26 (1983) 3553.
[16] W. A. Cooper, Plasma Phys. Control. Fusion 34 (1992) 1011.
[17] A. H. Grasser, J. M. Green and J. L. Johnson, Phys. Fluids 18 (1975) 143.
[18] S.Sakakibara et.al, proc. 31st EPS Conference on Plasma Phys. London, 28 June - 2 July 2004 ECA Vol.28B, O-4.01 (2004).
[19] U. Stroth et al, Nuclear Fusion 36 (1996) 1063.
[20] B.Peterson, et al., this conference
[21] Y.Nagayama, et a., this conference.
[22] N. Ohyabu, et al., *Phys. Rev. Lett.* 88, (2002) 55005.
[23] K. Narihara, et al., *Phys. Rev. Lett.* 87, (2001) 135002.
[24] K.Ida et al., *Phys. Rev. Lett.* 88, (2002) 015002.
[25] A.Komori, T.Morisaki, et al., this conference.
[26] T.Morisaki, et al., Fusion Eng. Design 65 (2003) 475.
[27] K.Ida, et. al., Phys Rev Lett 86 (2001) 5297.
[28] K.Ida, et. al., this conference
[29] L.M.Kovrizhnykh L.M. Nucl. Fusion 24 (1984) 435
[30] M.Yokoyama, et al., Nucl. Fusion 42 (2002) 143.
[31] S.Sudo et al, Nucl. Fusion 30 (1990) 11.
[32] Y.Takeiri, et al., this conference
[33] S.Morita, et al., Nucl. Fusion 43 (2003) 899.
[34] K.Tanaka, et al., this conference
[35] T.Shimozuma et al., this conference
[36] S.Sudo, N.Tamura, K.Khlopenkov,et al., Plasma Phys. Control. Fusion 44 (2002) 129.
[37] S. Inagaki, et al., *Phys. Rev. Lett.* 92 (2004) 55002.
[38] S. Inagaki, et al., Plasma Phys Control Fusion
[39] K.Ida et al., Plasma Phys Control Fusion 46 (2004) A45
[40] S. Inagaki, et al., this conference